High spin states in $^{135}_{57}La_{78}$

Ritika Garg,[1,*] S. Kumar,[1] Mansi Saxena,[1] Savi Goyal,[1] Davinder Siwal,[1] S. Verma,[1] R. Palit,[2] Sudipta Saha,[2] J. Sethi,[2] Sushil K. Sharma,[2] T. Trivedi,[2] S. K. Jadav,[2] R. Donthi,[2] B. S. Naidu,[2] and S. Mandal[1]

[1]*Department of Physics and Astrophysics, University of Delhi, Delhi - 110007, India*

[2]*Department of Nuclear and Atomic Physics, Tata Institute of Fundamental Research, Mumbai - 400005, India*

(Received 3 September 2012; revised manuscript received 11 January 2013; published 19 March 2013)

High spin states in ^{135}La have been investigated using the ^{128}Te(^{11}B,4n)^{135}La reaction at a beam energy of 50.5 MeV using the Indian National Gamma Array (INGA). The level scheme has been confirmed and extended both for low and high spin states with the observation of several new transitions. The Directional Correlations of Oriented states (DCO) ratios and linear polarization measurements have been performed to assign spin-parity for most of the reported γ transitions. A new positive parity band has been observed and identified as a decoupled band ($\Delta I = 2$). Two negative parity dipole bands ($\Delta I = 1$) have been established and for one of the dipole bands the crossover $E2$ transitions have been identified for the first time. On the basis of the Tilted Axis Cranking (TAC) calculations, a three quasiparticle (qp) $\pi(h_{11/2})^1 \otimes \nu(h_{11/2})^{-2}$ configuration and 5qp $\pi(h_{11/2})^1(g_{7/2}/d_{5/2})^2 \otimes \nu(h_{11/2})^{-2}$ configuration have been assigned to these two dipole bands. The comparison with experimental observables supports the configuration assignments for both the dipole bands.

DOI: 10.1103/PhysRevC.87.034317 PACS number(s): 21.10.Hw, 21.60.Ev, 23.20.Lv, 27.60.+j

I. INTRODUCTION

The nuclei near $A \sim 135$ with the neutron number approaching $N = 82$ shell closure show shape driving effects at high spins with moderate deformation and display a variety of interesting phenomena such as shape coexistence, magnetic rotation (MR), chiral rotation, dynamic symmetry in ^{134}Ba, and dynamic chirality in nuclei [1–10]. The Nilsson diagram indicates that there are several positive parity states originating from $g_{7/2}, d_{5/2}, d_{3/2}$, and $s_{1/2}$ shells and a negative parity state originating from the $h_{11/2}$ shell. For $N = 78$ odd-Z isotones, some of the dipole bands have been interpreted as MR bands [11,12] and a possible MR band crossing has been claimed [11,12]. However, in contrast to its isotones, the ^{135}La nucleus has not been explored and studied for such phenomenon. The present experimental work is, therefore, focused on the investigation of such high spin phenomena in this nucleus.

Previously, ^{135}La has been studied in radioactive decay [13–15]. The high spin structure of ^{135}La has been studied through the ^{128}Te(^{11}B,4n) reaction [16]. But complete information about the high spin structure of ^{135}La populated by the above reaction is limited. The low spin positive and negative parity bands have been predicted theoretically [17–21] and interpreted as arising from $d_{5/2}$, $g_{7/2}$, and $h_{11/2}$ orbitals. The structure of these bands have been interpreted as decoupled partners [21].

The present work reports on the reinvestigation of ^{135}La to search the high spin phenomena discovered in the last two decades [22]. The level scheme has been extended and confirmed both for low as well as high spin states and many new high spin states have been found. The experimental results obtained for high spin states are compared with the TAC calculations [23] to interpret the observed high spin dipole bands.

II. EXPERIMENTAL DETAILS

High spin states in ^{135}La were populated by the reaction ^{128}Te(^{11}B,4n)^{135}La using a ^{11}B beam of 50.5 MeV from the Pelletron Linac Facility at the Tata Institute of Fundamental Research (TIFR), Mumbai. The target consisted of 1.02 mg/cm^2 ^{128}Te on 4 mg/cm^2 ^{197}Au backing. The γ rays were detected using the INGA [24,25] spectrometer. In the current experiment, the array consisted of 16 Compton-suppressed clover detectors arranged in spherical geometry with 3, 2, 2, 4, 2, and 3 number of clover detectors placed at 157°, 140°, 115°, 90°, 65°, and 40° with respect to the beam direction, respectively. The detectors are placed at a distance of 25 cm from the target. The online data were collected via the XIA based triggerless Digital Data AcQuisition (DDAQ) system [24]. A total of about 3.9×10^9 two- and higher-fold events were recorded. The data were sorted using Multi pARameter time-stamped based COincidence Search program (MARCOS) to generate double and triple gamma coincidence matrices. The RADWARE software package was used for analysis of these matrices [26].

In order to obtain information about the multipolarities using the DCO method, an asymmetric matrix was created (using MARCOS) with the events detected at 90° clovers on one axis and 157° clovers on the other axis. The following relation was used for the calculation of DCO ratios:

$$R_{\mathrm{DCO}} = \frac{I^{\gamma_2}_{157^\circ}\left(\mathrm{gate}^{\gamma_1}_{90^\circ}\right)}{I^{\gamma_2}_{90^\circ}\left(\mathrm{gate}^{\gamma_1}_{157^\circ}\right)}. \quad (1)$$

The DCO ratios for a particular γ-ray transition were obtained by setting gates on stretched transitions of known multipolarity. When the gate is set on a stretched quadrupole transition, the ratio is close to 1.0 for a quadrupole and 0.5 for a dipole transition.

*ritikagarg25@gmail.com

The level parities were determined from the measurement of linear polarization of γ-ray transitions using the Integrated Polarizational Directional Correlation (IPDCO) method [27]. In this method the experimental asymmetry of Compton-scattered polarized photons is defined as

$$\Delta = \frac{a(E_\gamma)N_\perp - N_\parallel}{a(E_\gamma)N_\perp + N_\parallel}, \tag{2}$$

where $N_\perp$ and $N_\parallel$ denote the number of coincidence counts between the segments of the clover detectors in perpendicular and parallel direction to the emission plane, respectively [28]. The factor $a(E_\gamma)$ denotes the correction due to the asymmetry in response of the perpendicular and parallel clover segments. This factor was obtained from the analysis of the γ rays emitted by ^{152}Eu source placed at the target position and defined as

$$a(E_\gamma) = \frac{N_\parallel(\text{unpolarized})}{N_\perp(\text{unpolarized})}. \tag{3}$$

The value of $a(E_\gamma)$ for the detectors placed at an angle of 90° was found to be 1.005(3). For the analysis using the IPDCO method, two different asymmetric matrices with one axis corresponding to perpendicular or parallel scattered events in the detectors at 90° and other axis corresponding to all the detectors of the array were generated. Gates were set on the latter axis to get polarization asymmetry (Δ) from the intensity of the coincident perpendicular or parallel scattered gamma rays using Eq. (2). The experimental values of the asymmetry parameter (Δ) were obtained for several γ transitions as illustrated in Table I.

III. RESULTS

The level scheme of ^{135}La obtained from the present work as shown in Fig. 1 was constructed on the basis of γ-ray intensity considerations and coincidence relationships obtained from γ-γ and γ-γ-γ analysis. The present work has verified all the previously known levels [29] with certain changes and addition of new levels. The γ-ray energies, their relative intensities, $R_{\rm DCO}$, and linear polarization asymmetries obtained are listed in Table I. The intensities have been calculated from the total projection as well as by the gated spectra normalised with respect to 583 keV transition. The various bands obtained are assigned namely bands 1–10 as shown in Fig. 1. All the assigned parities of levels in the level scheme are extracted in the present work and confirmed for the previously known low spin states [16,29]. A typical γ-ray spectrum obtained with a gate on 583-keV transition is shown in Fig. 2.

A. Positive parity bands

1. Band numbers 1, 2, 3, and 4

Band 4 is the ground state band (Fig. 1) originating from the 5/2[413] Nilsson orbital [21]. It consists of 583-, 802-, and 920-keV transitions. The transitions of 120- and 464-keV connect band 3 to band 4 and band 4 to band 3, respectively. The $R_{\rm DCO}$ and polarization measurements of 802- and 920-keV confirmed their $E2$ character. The double gated coincidence spectra for bands 1, 2, and 3 are shown in the Fig. 3. Band 1 consists of 120-, 132-, 185-, 269-, 443-, and 368-keV transitions. 492.5-keV transition has been placed above 368-keV transition with tentative spin and parity assignment.

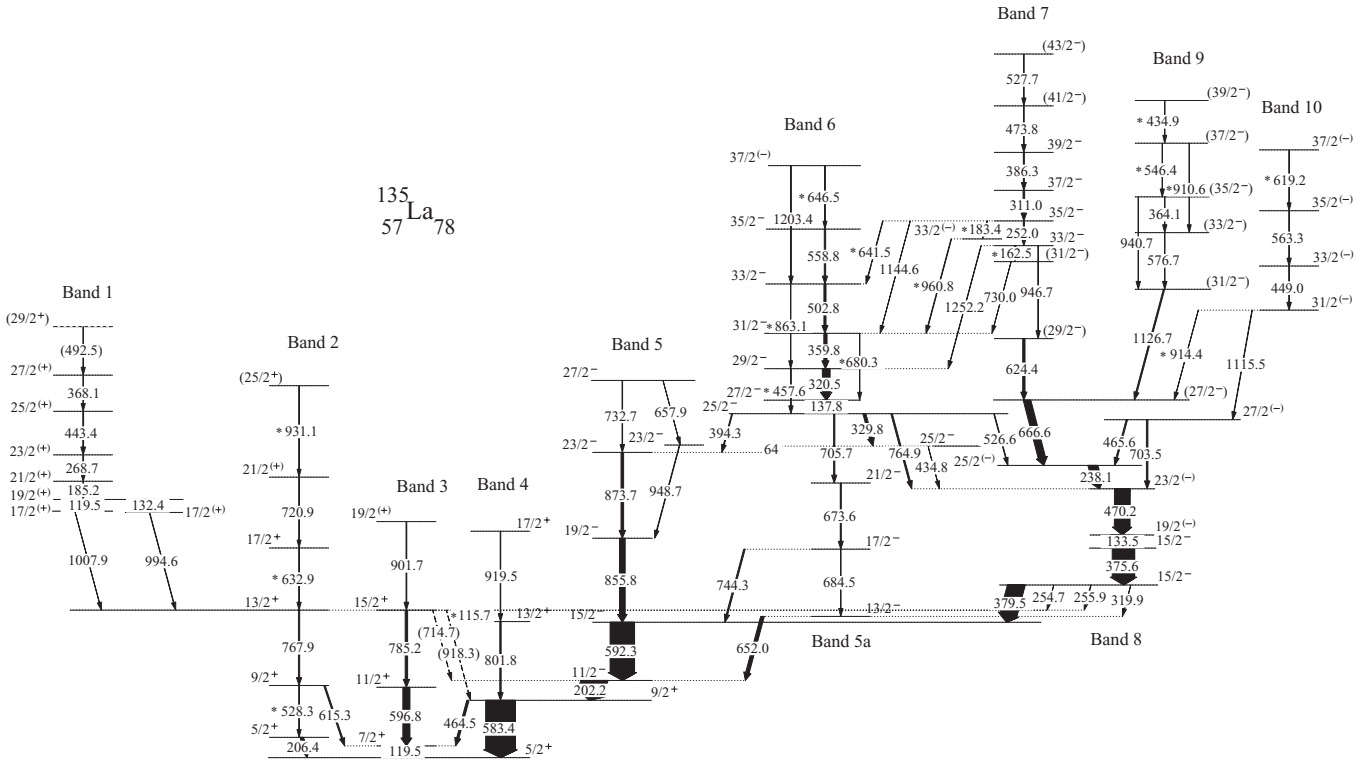

FIG. 1. The partial level scheme of ^{135}La deduced from the present work. New transitions are marked with an asterisk (*).

TABLE I. Level energy E_i, γ-ray energy E_γ, relative intensity I_γ, R_{DCO}, polarization asymmetry Δ, multipolarity and decay from initial spin J_i^π to final spin J_f^π for the γ-ray transitions in ^{135}La. Superscripts Q and D stand for the quadrupole and dipole nature of the gating transition in the determination of R_{DCO}.

E_i (keV)	E_γ (keV)	I_γ (rel.)	R_{DCO}	Δ	Multipolarity	$J_i^\pi \rightarrow J_f^\pi$
3171.5	64.0					$25/2^- \rightarrow 23/2^-$
1501.6	115.7	1.57(4)				$15/2^+ \rightarrow 13/2^+$
119.5	119.5		1.52(7)^Q		D	$7/2^+ \rightarrow 5/2^+$
2629.9	119.5	0.11(1)				$19/2^{(+)} \rightarrow 17/2^{(+)}$
	132.4		1.63(6)^D		D	$19/2^{(+)} \rightarrow 17/2^{(+)}$
2266.5	133.5	45.10(9)	1.72(6)^D		Q	$19/2^{(-)} \rightarrow 15/2^-$
3639.2	137.8	17.30(4)	0.60(3)^Q		D	$27/2^- \rightarrow 25/2^-$
5212.0	162.5		1.52(10)^D		D	$33/2^- \rightarrow (31/2^-)$
5464.1	183.4	0.40(2)	1.62(12)^D		D	$35/2^- \rightarrow 33/2^{(-)}$
2815.1	185.2		0.66(2)^Q		D	$21/2^{(+)} \rightarrow 19/2^{(+)}$
785.6	202.2	86.90(15)	0.80(2)^Q	0.28(2)	$E1$	$11/2^- \rightarrow 9/2^+$
206.4	206.4		1.59(9)^Q			$5/2^+ \rightarrow 5/2^+$
2974.8	238.1	29.90(5)	1.17(5)^D		D	$25/2^{(-)} \rightarrow 23/2^{(-)}$
5464.1	252.0	3.51(5)	1.09(4)^D		D	$35/2^- \rightarrow 33/2^-$
1757.3	254.7	0.30(1)				$15/2^- \rightarrow 13/2^+$
1757.3	255.9	1.53(2)				$15/2^- \rightarrow 15/2^+$
3083.8	268.7	2.40(4)	0.61(2)^Q		D	$23/2^{(+)} \rightarrow 21/2^{(+)}$
5775.1	311.0	5.17(8)	0.47(2)^Q	−0.04(3)	$M1$	$37/2^- \rightarrow 35/2^-$
1757.3	319.9					$15/2^- \rightarrow 13/2^-$
3959.7	320.5	24.80(8)	0.48(2)^Q	−0.06(2)	$M1$	$29/2^- \rightarrow 27/2^-$
3501.4	329.8	9.47(11)	0.63(2)^Q	−0.07(3)	$M1$	$25/2^- \rightarrow 25/2^-$
4319.5	359.8	10.50(2)	0.46(1)^Q	−0.03(2)	$M1$	$31/2^- \rightarrow 29/2^-$
5708.8	364.1	1.10(2)	0.60(5)^Q		D	$(35/2^-) \rightarrow (33/2^-)$
3895.4	368.1	0.61(4)	0.99(5)^D	−0.30(8)	$M1$	$27/2^{(+)} \rightarrow 25/2^{(+)}$
2132.9	375.6	74.30(11)	1.11(3)^Q	0.18(1)	$\Delta I = 0$	$15/2^- \rightarrow 15/2^-$
1757.3	379.5	57.0(6)	1.07(3)^Q	0.19(2)	$\Delta I = 0$	$15/2^- \rightarrow 15/2^-$
6161.4	386.3	3.43(3)	0.81(3)^D	−0.04(3)	$M1$	$39/2^- \rightarrow 37/2^-$
3501.4	394.3	2.84(4)	0.47(2)^Q		D	$25/2^- \rightarrow 23/2^-$
3171.5	434.8					$25/2^- \rightarrow 23/2^{(-)}$
6690.2	434.9	0.49(4)	0.37(5)^Q		D	$(39/2^-) \rightarrow (37/2^-)$
3527.3	443.4	1.80(3)	0.46(3)^Q		D	$25/2^{(+)} \rightarrow 23/2^{(+)}$
5005.0	449.0	1.93(3)	0.48(3)^Q		D	$33/2^{(-)} \rightarrow 31/2^{(-)}$
3959.7	457.6	1.25(2)	1.97(9)^Q		Q	$29/2^- \rightarrow 25/2^-$
583.4	464.5	7.47(14)				$9/2^+ \rightarrow 7/2^+$
3440.4	465.6	4.30(5)	0.41(2)^Q	−0.16(5)	$M1$	$27/2^{(-)} \rightarrow 25/2^{(-)}$
2736.9	470.2	52.1(5)	1.04(4)^D	0.03(1)	Q + D	$23/2^{(-)} \rightarrow 19/2^{(-)}$
6635.3	473.8	2.05(3)				$(41/2^-) \rightarrow 39/2^-$
4387.9	492.5	0.78(2)				$(29/2^+) \rightarrow 27/2^{(+)}$
4822.3	502.8	6.95(7)	0.47(2)^Q	−0.08(4)	$M1$	$33/2^- \rightarrow 31/2^-$
3501.4	526.6					$25/2^- \rightarrow 25/2^{(-)}$
734.7	528.3	0.78(2)	1.12(9)^Q	0.04(2)	$E2$	$9/2^+ \rightarrow 5/2^+$
7163.0	527.7					$(43/2^-) \rightarrow (41/2^-)$
6255.4	546.4	0.74(4)	0.35(3)^Q		D	$(37/2^-) \rightarrow (35/2^-)$
5381.1	558.8	4.49(5)	0.32(1)^Q	−0.12(2)	$M1$	$35/2^- \rightarrow 33/2^-$
5568.2	563.3	1.24(2)	0.38(2)^Q		D	$35/2^{(-)} \rightarrow 33/2^{(-)}$
5344.9	576.6	1.66(3)	0.38(2)^Q	−0.35(6)	$M1$	$(33/2^-) \rightarrow (31/2^-)$
583.4	583.4	100.0(13)	1.06(3)^Q	0.08(5)	$E2$	$9/2^+ \rightarrow 5/2^+$
1377.9	592.3	82.6(8)	1.00(3)^Q	0.09(1)	$E2$	$15/2^- \rightarrow 11/2^-$
716.3	596.8	23.9(3)	1.29(4)^Q	0.13(3)	$E2$	$11/2^+ \rightarrow 7/2^+$
734.7	615.3	4.44(6)	0.61(2)^Q		D	$9/2^+ \rightarrow 7/2^+$
6187.4	619.2	0.32(1)	0.95(8)^D		D	$37/2^{(-)} \rightarrow 35/2^{(-)}$
4266.0	624.4	7.71(10)	0.35(2)^Q	−0.07(2)	$M1$	$(29/2^-) \rightarrow (27/2^-)$
2135.6	632.9	1.00(3)	0.95(7)^Q	0.13(5)	$E2$	$17/2^+ \rightarrow 13/2^+$
5464.1	641.5	1.53(8)	0.84(5)^D	−0.14(5)	$M1$	$35/2^- \rightarrow 33/2^-$
6027.6	646.5	0.34(1)				$37/2^{(-)} \rightarrow 35/2^-$
1437.6	652.0	11.98(16)	0.37(1)^Q	0.05(2)	D + Q	$13/2^- \rightarrow 11/2^-$

TABLE I. (*Continued.*)

E_i (keV)	E_γ (keV)	I_γ (rel.)	R_{DCO}	Δ	Multipolarity	$J_i^\pi \rightarrow J_f^\pi$
3840.2	657.9	0.37(2)	0.94(9)[Q]		Q	$27/2^- \rightarrow 23/2^-$
3641.6	666.6	25.0(3)	1.08(4)[Q]	−0.09(2)		$(27/2^-) \rightarrow 25/2^{(-)}$
2795.7	673.6	3.58(5)	0.84(4)[Q]	0.13(3)	$E2$	$21/2^- \rightarrow 17/2^-$
4319.5	680.3	0.44(4)				$31/2^- \rightarrow 27/2^-$
2122.1	684.5	1.19(23)	1.09(5)[Q]	0.13(4)	$E2$	$17/2^- \rightarrow 13/2^-$
3440.4	703.5	4.97(6)	1.14(4)[Q]	0.16(2)	Q	$27/2^{(-)} \rightarrow 23/2^{(-)}$
3501.4	705.7	4.11(16)	0.95(5)[Q]	0.32(5)	$E2$	$25/2^- \rightarrow 21/2^-$
1501.6	714.7	0.89(3)				$15/2^+ \rightarrow 11/2^-$
2856.5	720.9	0.34(1)	1.39(8)[Q]		Q	$21/2^{(+)} \rightarrow 17/2^+$
5049.5	730.0					$(31/2^-) \rightarrow 31/2^-$
3840.2	732.7	1.77(4)	1.12(6)[Q]	0.13(4)	$E2$	$27/2^- \rightarrow 23/2^-$
2122.1	744.3	4.74(6)		−0.06(2)	M	$17/2^- \rightarrow 15/2^-$
3501.4	764.9	4.95(5)	0.50(2)[Q]	0.15(3)	$D+Q$	$25/2^- \rightarrow 23/2^{(-)}$
1502.6	767.9	4.20(6)	2.08(11)[D]	0.09(4)	$E2$	$13/2^+ \rightarrow 9/2^+$
1501.6	785.2	8.17(11)	0.90(4)[Q]	0.08(2)	$E2$	$15/2^+ \rightarrow 11/2^+$
1385.2	801.8	4.48(6)	0.84(4)[Q]	0.08(3)	$E2$	$13/2^+ \rightarrow 9/2^+$
2233.6	855.8	19.33(18)	0.97(4)[Q]	0.08(2)	$E2$	$19/2^- \rightarrow 15/2^-$
4822.3	863.1	0.22(3)	1.59(24)[D]		Q	$33/2^- \rightarrow 29/2^-$
3107.3	873.7	8.75(11)	1.00(4)[Q]	0.12(3)	$E2$	$23/2^- \rightarrow 19/2^-$
2403.3	901.7	2.47(4)	0.93(5)[Q]		Q	$19/2^{(+)} \rightarrow 15/2^+$
6255.4	910.6	0.15(6)				$(37/2^-) \rightarrow (33/2^-)$
4556.0	914.4	0.71(2)				$31/2^{(-)} \rightarrow (27/2^-)$
1501.6	918.3	0.54(2)				$15/2^+ \rightarrow 9/2^+$
2304.7	919.5	1.80(2)	0.92(9)[Q]	0.07(3)	$E2$	$17/2^+ \rightarrow 13/2^+$
3787.7	931.1	0.06(1)				$(25/2^+) \rightarrow 21/2^{(+)}$
5708.8	940.7	1.47(4)	1.04(10)[Q]		Q	$(35/2^-) \rightarrow (31/2^-)$
5212.0	946.7	1.29(4)				$33/2^- \rightarrow (29/2^-)$
3182.3	948.7	1.78(3)	0.96(6)[Q]	0.09(5)	$E2$	$23/2^- \rightarrow 19/2^-$
5280.4	960.8	1.91(2)				$33/2^{(-)} \rightarrow 31/2^-$
2497.3	994.6	1.46(4)	0.89(6)[Q]		Q	$17/2^{(+)} \rightarrow 13/2^+$
2510.5	1007.9	0.83(3)	0.84(8)[Q]		Q	$17/2^{(+)} \rightarrow 13/2^+$
4556.0	1115.4	1.49(7)	1.02(11)[Q]		Q	$31/2^{(-)} \rightarrow 27/2^{(-)}$
4768.2	1126.7	4.28(5)	1.22(8)[Q]	−0.02(3)	Q	$(31/2^-) \rightarrow (27/2^-)$
5464.1	1144.6	0.63(1)	0.96(8)[Q]		Q	$35/2^- \rightarrow 31/2^-$
6027.6	1203.4	1.75(4)	0.92(6)[Q]		Q	$37/2^{(-)} \rightarrow 33/2^-$
5212.0	1252.2	1.14(2)	1.88(18)[D]	0.05(3)	$E2$	$33/2^- \rightarrow 29/2^-$

Band 1 decays to band 2 through the transitions 995 and 1008 keV. These transitions have been identified as quadrupole in nature on the basis of R_{DCO} measurements. Band 2 has been observed for the first time in the present work. The R_{DCO} and polarization measurements of 528-, 768-, and 633-keV transitions of band 2 confirmed their $E2$ character. The in-band 721 keV has been assigned as quadrupole from the R_{DCO} measurements. Band 3 consists of 597-, 785-, and 902-keV transitions with linking transitions of 116, 715, and 918 keV to the $13/2^+$ level of band 4, $11/2^-$ level of band 5 and $9/2^+$ level of band 4, respectively. Spin and parity of this band have been assigned on the basis of R_{DCO} and polarization measurements as given in Table I. However, the energy levels 1502.6 keV and 1501.6 keV decay via 768-and 785-keV transitions, respectively, and these are different levels because of absence of 902-keV transition in Fig. 3(a). This suggests that the levels $13/2^+$ and $15/2^+$ are not degenerate and that defines a different level for the transitions and explains the placement of 206-, 528-, 768-, 633-, 721-, and 931-keV transitions in band 2.

B. Negative parity bands

1. Band numbers 5, 6, and 7

Band 5 decays to band 4 via 202 keV transition which is $E1$ as determined from R_{DCO} and polarization measurements. The in-band transitions of this band consist of the 592-, 856-, 874-, and 733-keV transitions. The placement of the γ rays is confirmed from the coincidence and relative intensity measurements and the multipolarities determined on the basis of R_{DCO} and polarization measurements. The transitions 592-, 856-, 874, and 733-keV have been assigned as $E2$ and the assigned quadrupole nature of the 658-keV transition is also consistent with the previous reported work [16,29]. The linking transitions 652 and 744 keV connect band 5 and sideband 5a. This sideband contains 685-, 674-, and 706-keV transitions which have been assigned $E2$ character. Band 5 is interconnected to band 6 through a 394-keV transition.

Band 6 is built on 3501.4 keV ($I^\pi = 25/2^-$) level and consists of 138-, 320-, 360-, 503-, 559-, and 646-keV

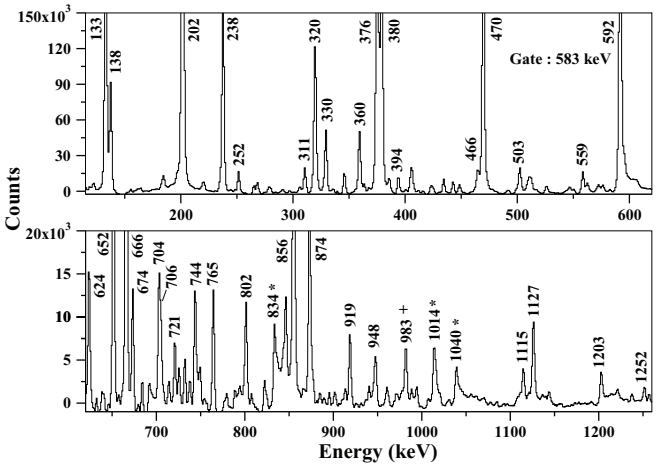

FIG. 2. γ-γ coincidence spectrum gated by the 583 keV $9/2^+ \rightarrow 5/2^+$ γ-ray transition. The contaminant transitions are marked with an asterisk ($*$). The peak at 983-keV marked with a plus sign is not placed in level scheme. Its origin is unknown.

($\Delta I = 1$) transitions along with weak crossover 458-, 680- [Fig. 4(a)], 863-, and 1203-keV transitions [Fig. 4(b)]. The crossover transitions 458 and 680 keV have been identified for the first time. A new transition of 646 keV ($\Delta I = 1$) has been placed at the top of this band extending the excitation energy of the band to 6027.6 keV. The band-head spin $I^\pi = 25/2^-$ of this band was obtained from the multipolarity of 706-keV transition (sideband 5a). The R_{DCO} and polarization measurement of 706-keV transition has been deduced by the gated spectrum of 674 keV. The result of R_{DCO} and polarization measurement confirms the $M1$ character of the in-band 320-, 360-, 503-, and 559-keV transitions. The 1203-keV crossover transition has been assigned multipolarity as quadrupole based on R_{DCO} measurements. This band decays to band 8 via 527-, 765-, and 330-keV transitions.

A new transition of 162-keV has been observed and placed as the lowest transition in band 7. The other transitions of this band are 252, 311, 386, 474, and 528 keV (Fig. 5). The

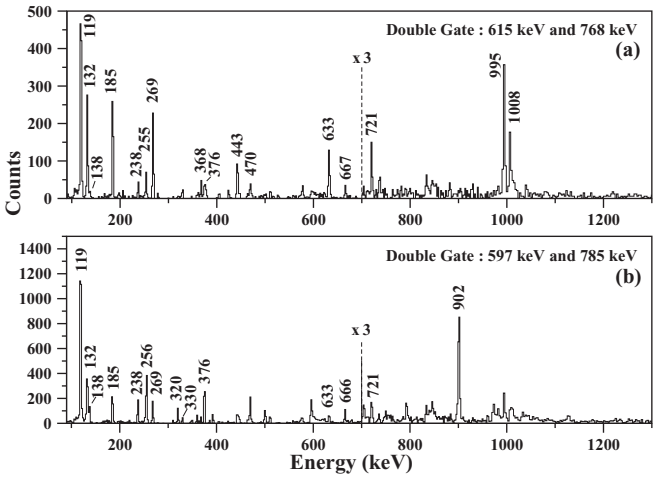

FIG. 3. Double gated coincidence spectra showing the transitions of bands 1, 2, and 3.

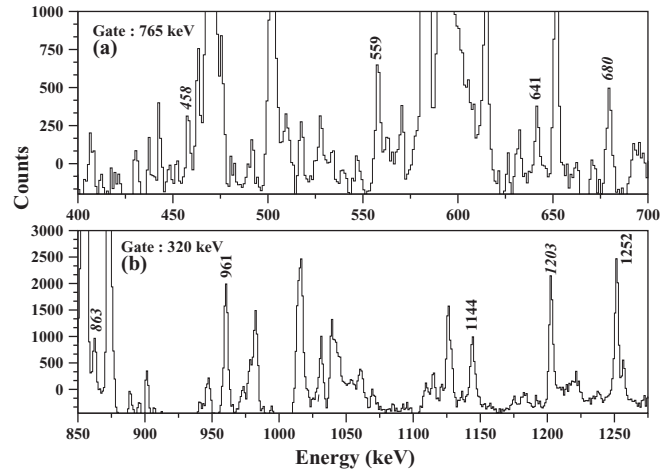

FIG. 4. Coincidence spectra showing crossover transitions (marked in italics) in band 6.

R_{DCO} value of 252 keV suggest that this transition is dipole. R_{DCO} and polarization measurements of 311- and 386-keV transitions suggest that these are $M1$. The 183-, 641-, and 961-keV transitions [Fig. 5(a)] that decay out to band 6 have been observed for the first time. The multipolarity extracted for the 641-keV transition suggests its $M1$ character and is used to assign further spin and parity of band 7. The other linking transitions between bands 6 and 7 are shown in Fig. 5.

2. *Band numbers 8, 9, and 10*

Band 8 is fairly strong and is found to decay to the $13/2^+$ level at 1502.6 keV (band 2) and $15/2^+$ level at 1501.6 keV (band 3) via 255- and 256-keV transitions from the $15/2^-$ level at 1757.3 keV. The transitions 376 and 380 keV have R_{DCO} values 1.11 and 1.07 along with polarization asymmetry values 0.18 and 0.19, respectively. However, these values are not consistent with $E2(\Delta I = 2)$, $E1$, and $M1$ character (see Table I). The polarization asymmetry value can distinguish

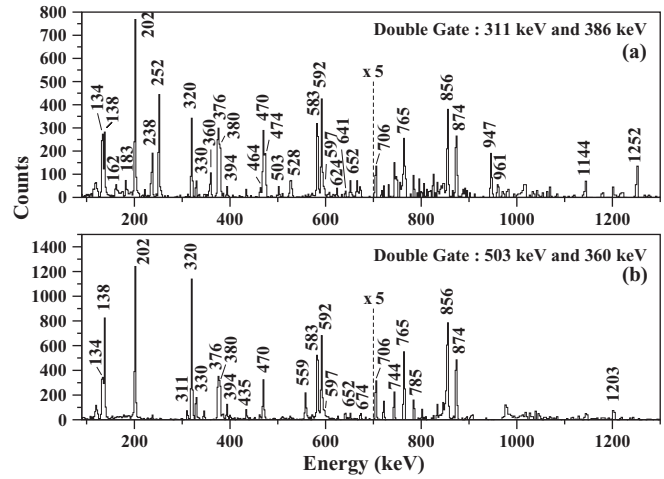

FIG. 5. Double gated coincidence spectra shows the transitions belonging to the negative parity dipole bands 6 and 7 along with the interconnecting transitions to other bands.

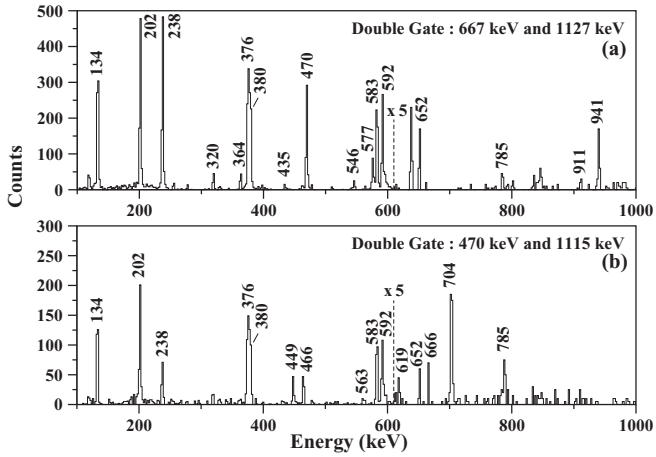

FIG. 6. Double gated coincidence spectra showing the γ-ray transitions of bands 9 and 10.

$\Delta I = 0$ mixed transition from stretched quadrupole transition [30]. Therefore, on the basis of observed similar $R_{\rm DCO}$ and polarisation values, the transitions 376 and 380 keV have been assigned $\Delta I = 0$ character. The structure of the two $15/2^-$ states can arise from the coupling of one proton in $g_{7/2}/d_{5/2}$ orbitals with two neutrons in $h_{11/2}$ and $d_{3/2}$, respectively.

Generally at high spins, stretched transitions are much more intense than nonstretched transitions. The observation of high intensity for 376- and 380-keV transitions can favor stretched nature over unstretched nature. But this assignment will lead to contradiction of band-head spin of band 6 which has been established by 706-keV transition of band 5a. Hence, our present assignment also supports the band-head spin of band 6. Band 9 consists of 577-, 364-, 546-, and 435-keV transitions along with the crossover transitions of 941 and 911 keV [Fig. 6(a)]. This band decays to band 8 via 1127-keV transition. The cascade with transitions 449, 563, and 619 keV represents band 10 [Fig. 6(b)]. The $R_{\rm DCO}$ values of 449, 563, and 619 keV suggest that these are dipole transitions. The transition of 619 keV has been observed for the first time extending the excitation energy of the band to 6187.2 keV. The intensities of the transitions in this band are not sufficient to determine their parities, so the parity assignment of the levels in band 10 remains tentative. Band 10 decays through the newly observed 914-keV transition to the level at 3641.4 keV in band 7. The interband transition of 1115 keV connecting band 10 to band 8 at 3440.4-keV level has $R_{\rm DCO}$ value = 1.02 which suggests that the transition is quadrupole in nature.

IV. DISCUSSION

Figure 7 shows the systematics of the bands based on the $\pi h_{11/2}$ configuration in the odd mass lanthanum isotopes. The energy level spacings across the series of La isotopes reflect the decrease of quadrupole deformation as the neutron number increases. As the neutron number increases and approaches towards $N = 82$ irregular band structures start to dominate. Among lower spin states a new positive parity band called band 2 has been established. This band has been identified as

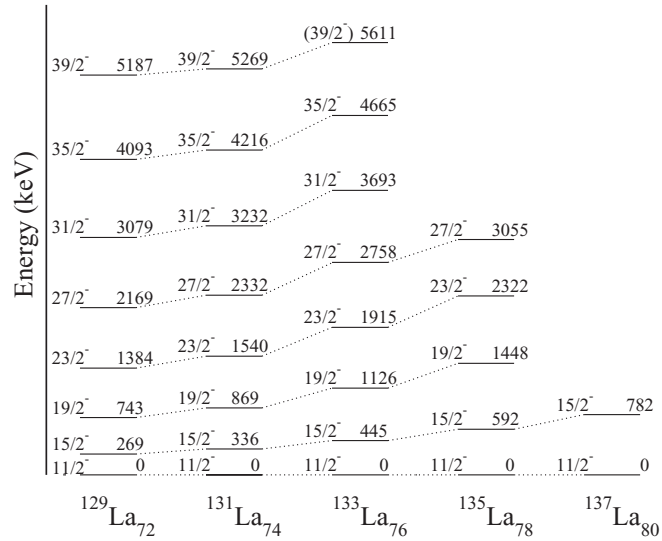

FIG. 7. The bands based on $11/2^-$ states in the odd mass lanthanum isotopes.

the decoupled partner of the $g_{7/2}$ band for the first time in this nucleus, and is similar to that observed in the neighbouring nucleus ^{133}La [31]. Figure 8 shows that the energy level spacings of three positive parity bands (bands 2, 3, and 4) in ^{135}La are very similar to those of the $2^+ \rightarrow 0^+$, $4^+ \rightarrow 2^+$, and $6^+ \rightarrow 4^+$ transitions in the even-even core nucleus ^{134}Ba.

The identification and placement of negative parity dipole bands (bands 6 and 7) is the focus of the present study. The experimental data for these negative parity dipole bands have been compared with the TAC model calculations [23]. This hybrid version of the TAC model combines a spherical Woods-Saxon potential with a deformed Nilsson potential. In our calculations for the bands 6 and 7, the pairing gap parameters were chosen to be 0.8 times the experimental

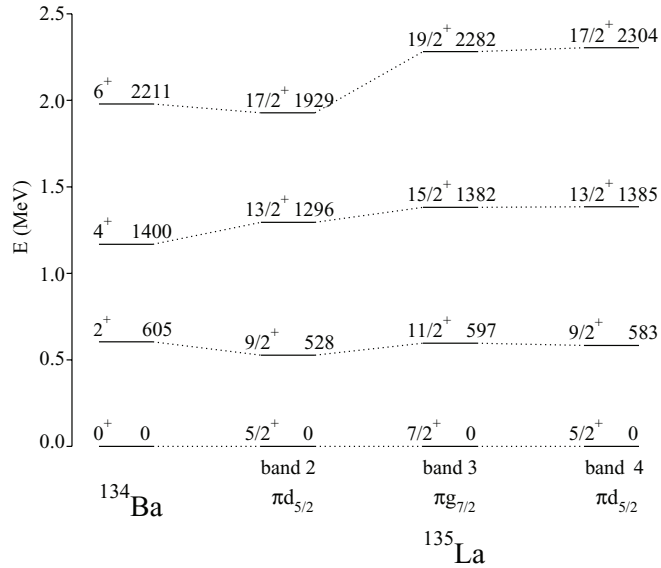

FIG. 8. The energy levels of the bands in ^{135}La, compared with the ground band of the neighbouring even-even nucleus ^{134}Ba.

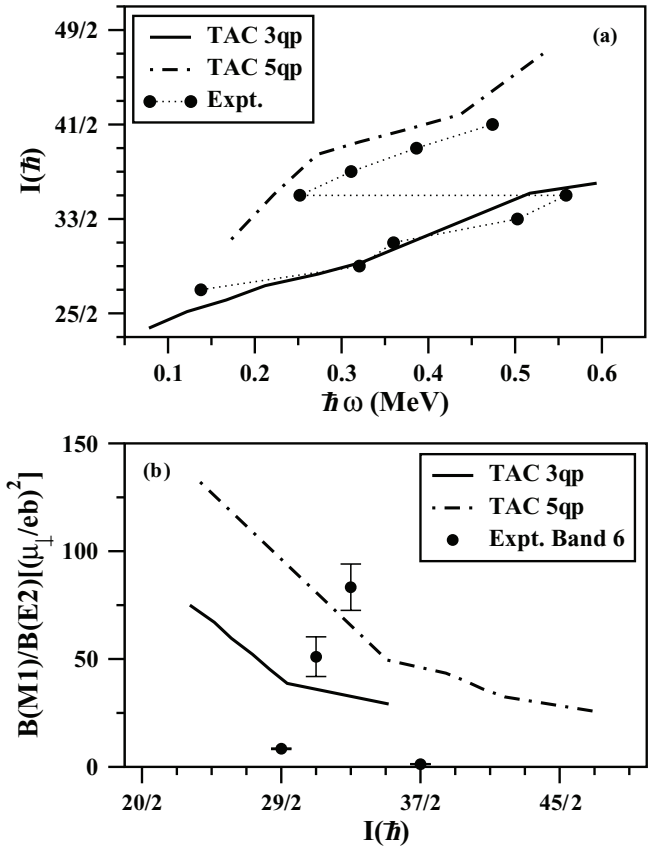

FIG. 9. Upper panel shows $I(\hbar)$ vs $\hbar\omega$ of band 6 and 7. Lower panel shows variation of $B(M1)/B(E2)$ as a function of $I(\hbar)$ for band 6.

even-odd mass difference, i.e., $\Delta_p = 1.059$ MeV and $\Delta_n = 0.748$ MeV. On the basis of the systematics of $N = 78$ isotones, a three-quasiparticle (3qp) configuration $\pi(h_{11/2})^1 \otimes \nu(h_{11/2})^{-2}$ has been assigned to band 6. This configuration resulted in a minimum in the total energy at a deformation of $\epsilon_2 = 0.120$, $\gamma = 58^\circ$ with an average tilt angle $\theta = 31.1^\circ$. A five-quasiparticle (5qp) configuration $\pi(h_{11/2})^1(g_{7/2}/d_{5/2})^2 \otimes \nu(h_{11/2})^{-2}$ has been considered for band 7. This configuration resulted in a minimum in the total energy at a deformation of $\epsilon_2 = 0.116$, $\gamma = 60^\circ$ with a average tilt angle $\theta = 29.8^\circ$. Strutinsky's minimization [32] was obtained at $\hbar\omega = 0.25$ and 0.15 MeV for both the configurations. The theoretical $B(M1)$ values show a decrease with increase of the spin for bands 6 and 7, and strongly suggests MR phenomenon.

Figure 9(a) compares the experimental spin I($\hbar$) versus $\hbar\omega$ for bands 6 and 7 with the TAC calculations. It is clear that the theoretical calculation for 3qp and 5qp configurations reproduces the angular momentum behaviour observed for bands 6 and 7, respectively. The figure also depicts a band crossing at $\hbar\omega \approx 0.41$ MeV. In Fig. 9(b) the theoretical $B(M1)/B(E2)$ ratios along with a comparison with experimental data are presented. The experimental $B(M1)/B(E2)$ ratios show an increase with increase of spin up to $I = 33/2$. After this there is a decrease in the ratio with increase of spin. This behavior shows a change in the configuration at $I = 33/2$. The experimental data (crossover $E2$ transitions)

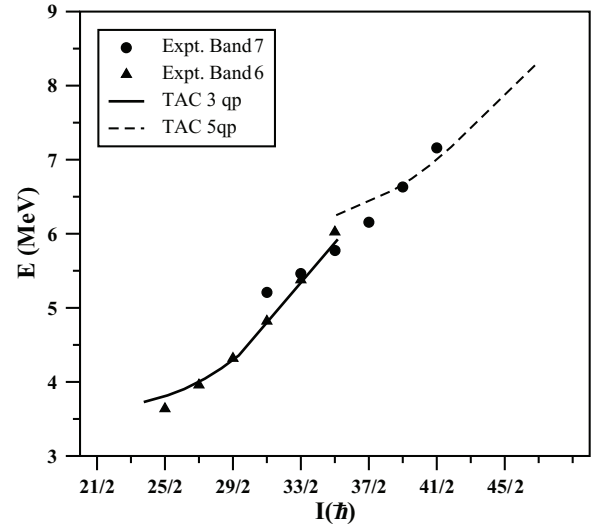

FIG. 10. Energy vs spin $I(\hbar)$ for bands 6 and 7 along with TAC calculations.

is not sufficient at higher spins for a proper comparison of $B(M1)/B(E2)$ ratios of bands 6 and 7 with TAC calculations. Figure 10 shows the plot of excitation energy versus spin for the negative parity dipole bands. The experimental data show a band crossing between bands 6 and 7 at a spin of $I \approx 33/2^-\,\hbar$. The theoretical calculations (TAC) reproduce the trend of the experimental observations but the bands cross at $I \approx 35/2^-\,\hbar$. There is a good agreement between the theoretical results of the 3qp configuration with the experimental data of band 6. The theoretical calculations for 5qp configuration reproduce the experimental data for band 7 [Figs. 9(a) and 10].

The agreement of the theoretical calculations with the experimental data leads to the assignment of 3qp configuration $\pi(h_{11/2})^1 \otimes \nu(h_{11/2})^{-2}$ to the lower part of band 6 and 5qp configuration $\pi(h_{11/2})^1(g_{7/2}/d_{5/2})^2 \otimes \nu(h_{11/2})^{-2}$ to band 7.

V. SUMMARY AND CONCLUSION

High spin states of ^{135}La have been studied through the ^{128}Te(^{11}B,4n)^{135}La reaction at a beam energy of 50.5 MeV. The earlier known level scheme has been confirmed. Many new gamma transitions have been observed in the present work and placed in the level scheme. Spin-parity has been assigned to the levels on the basis of multipolarities of transitions from DCO and IPDCO measurements. A positive parity band ($\Delta I = 2$) has been established and identified as a decoupled band. Two negative parity dipole bands have been observed and interpreted in the framework of TAC model. One of the dipole bands (band 6) has been extended to a spin of $37/2^-$ and excitation energy of 6028 keV. Two crossover $E2$ transitions have been observed for the first time in this band. A band crossing has been seen between bands 6 and 7. Experimental data has been compared with TAC calculations. On the basis of this comparison, 3qp configuration $\pi(h_{11/2})^1 \otimes \nu(h_{11/2})^{-2}$ and 5qp configuration $\pi(h_{11/2})^1(g_{7/2}/d_{5/2})^2 \otimes \nu(h_{11/2})^{-2}$ have been assigned to bands 6 and 7, respectively. TAC calculations suggest MR features for the dipole bands 6 and 7. However,

lifetime measurements may be required to support the confirmation of the MR nature of these bands.

ACKNOWLEDGMENTS

The authors gratefully acknowledge the support provided by the staff of TIFR-BARC pelletron facility, the target laboratory staff at TIFR, the INGA collaboration and the Department of Science and Technology, India, for providing funds for the INGA project (No. IR/S2/PF-03/2003-I). We would like to thank Prof. S. C. Pancholi for the discussions and his views and comments. This work was performed under collaborative research scheme no. CRS/2009/NP02/1350 of UGC-DAE Consortium for Scientific Research. R.G. would like to acknowledge CSIR, India, for financial assistance.

[1] S. Kumar *et al.*, Phys. Rev. C **81**, 067304 (2010).
[2] E. S. Paul, D. B. Fossan, Y. Liang, R. Ma, and N. Xu, Phys. Rev. C **40**, 1255 (1989).
[3] C. M. Petrache, G. de Angelis, D. Bucurescu, M. Ivascu, D. Bazzacco, and S. Lunardi, Z. Phys. A **344**, 227 (1992).
[4] S. Kumar, R. Palit, H. C. Jain, I. Mazumdar, P. K. Joshi, S. Roy, A. Y. Deo, Z. Naik, S. S. Malik, and A. K. Jain, Phys. Rev. C **76**, 014306 (2007).
[5] S. Lakshmi, H. C. Jain, P. K. Joshi, A. K. Jain, and S. S. Malik, Phys. Rev. C **69**, 014319 (2004).
[6] S. Mukhopadhyay *et al.*, Phys. Rev. C **78**, 034311 (2008).
[7] K. Starosta, C. J. Chiara, D. B. Fossan, T. Koike, T. T. S. Kuo, D. R. LaFosse, S. G. Rohoziński, Ch. Droste, T. Morek, and J. Srebrny, Phys. Rev. C **65**, 044328 (2002).
[8] R. F. Casten and N. V. Zamfir, Phys. Rev. Lett. **85**, 3584 (2000).
[9] D. Tonev *et al.*, Phys. Rev. Lett. **96**, 052501 (2006).
[10] S. C. Pancholi, *Exotic Nuclear Excitations* (Springer, New York, 2011).
[11] P. Agarwal *et al.*, Phys. Rev. C **76**, 024321 (2007).
[12] A. Dhal *et al.*, Phys. Rev. C **80**, 014320 (2009).
[13] S. Morinobu, T. Hirose, and K. Hisatake, Nucl. Phys. **61**, 613 (1965).
[14] A. Abdul-Malek and R. A. Naumann, Phys. Rev. **166**, 1194 (1968).
[15] E. A. Henry and R. A. Meyer, Phys. Rev. C **12**, 1321 (1975).
[16] N. Xu, Ph.D. thesis, State University, New York, 1990.
[17] J. R. Leigh, K. Nakai, K. H. Maier, F. Pühlhofer, F. S. Stephens, and R. M. Diamond, Nucl. Phys. A **213**, 1 (1973).
[18] A. Ikeda, Phys. Rev. C **24**, 1656 (1981).
[19] C. E. Alonso, J. M. Arias, and M. Lozano, J. Phys. G **13**, 1269 (1987).
[20] L. Y. Jia, H. Zhang, and Y. M. Zhao, Phys. Rev. C **76**, 054305 (2007).
[21] C. Junsei, R. S. Hayano, M. Sekimoto, H. Nakayama, and K. Nakai, J. Phys. Soc. Jpn. **43**, 1109 (1977).
[22] S. Frauendorf, Rev. Mod. Phys. **73**, 463 (2001).
[23] V. I. Dimitrov, F. Dönau, and S. Frauendorf, Phys. Rev. C **62**, 024315 (2000).
[24] R. Palit *et al.*, Nucl. Instrum. Methods Phys. Res. A **680**, 90 (2012).
[25] R. Palit, AIP Conf. Proc. **1336**, 573 (2011).
[26] D. C. Radford, Nucl. Instrum. Methods Phys. Res. A **361**, 297 (1995).
[27] K. Starosta *et al.*, Nucl. Instrum. Methods Phys. Res. A **423**, 16 (1999).
[28] R. Palit, H. C. Jain, P. K. Joshi, S. Nagaraj, B. V. T. Rao, S. N. Chintalapudi, and S. S. Ghugre, Pramana **54**, 347 (2000).
[29] NNDC Online Data Service, http://www.nndc.bnl.gov
[30] J. A. Grau, L. E. Samuelson, F. A. Rickey, P. C. Simms, and G. J. Smith, Phys. Rev. C **14**, 2297 (1976).
[31] T. Morek, H. Beuscher, B. Bochev, D. R. Haenni, T. Kutsarova, R. M. Lieder, M. Müller-Veggian, and A. Neskakis, Nucl. Phys. A **391**, 269 (1982).
[32] V. M. Strutinsky, Nucl. Phys. A **95**, 420 (1967).